International Journal of Microwave and Wireless Technologies

cambridge.org/mrf

Compact eight-channel diplexer based on quad-mode stepped impedance resonator

Kaijun Song[1,2], Lele Fang[1,2], Qian Li[1,2] and Yong Fan[1,2]

[1]Yangtze Delta Region Institute (Huzhou), University of Electronic Science and Technology of China, Huzhou, China and [2]EHF Key Laboratory of Fundamental Science, School of Electronic Science and Engineering, University of Electronic Science and Technology of China, Chengdu, China.

Research Paper

Cite this article: Song K, Fang L, Li Q, Fan Y (2024) Compact eight-channel diplexer based on quad-mode stepped impedance resonator. *International Journal of Microwave and Wireless Technologies* **16**(10), 1713–1721. https://doi.org/10.1017/S1759078724000540

Received: 26 December 2023
Revised: 24 April 2024
Accepted: 29 April 2024

Keywords:
bandpass filter; compact; eight-channel diplexer; quad-mode stepped impedance resonator (QMSIR)

Corresponding author: Kaijun Song;
Email: ksong@uestc.edu.cn

Abstract

A compact microstrip eight-channel diplexer based on quad-mode stepped impedance resonator (QMSIR) is proposed in this paper. The proposed diplexer is composed by two second-order quad-band bandpass filters (BPFs) and common-port distributed coupling matching circuit. Each quad-band BPF is formed by two coupled-QMSIRs controlling the passband characteristics. By introducing multiple coupling paths between input and output ports, the isolation between the eight channels is performed. For demonstration, an eight-channel diplexer based on QMSIR is designed and fabricated with microstrip technology. The use of the QMSIR can lead to significant size reduction for the multiplexer, this is because the required resonator number is reduced. As a result, the diplexer occupies a compact size of $0.083\lambda^2$, which is smaller than most of the eight-channel diplexers that have been proposed. And the 3 dB fractional bandwidth is 97% (2.5–7.2 GHz). Measurement results correlate well with the simulated predictions, showing that a good isolation of better than 20 dB and upper stopband of better than 10 dB.

Introduction

In recent years, the microwave passive circuits are being considered as one of the crucial research areas for advanced handset applications. Recently, the microwave filters and multi-band circuits were realized by using different technique [1–10]. Today, much research is interested on the realization of multiplexer modules with multichannel, small size/volume and low cost by embedding passive components into PCB substrates. The most well-known method to design the planar diplexers is to combine the bandpass filters (BPFs) with an associated matching circuit. By using this method, many diplexers and multiplexers are designed [11–20]. It is getting challenging as the channel number increases. To reduce circuit size, in paper [11], a design technique of high performance diplexer for multi-wireless networks based on multilayered U-shape resonators was presented. In paper [12], a new structure for diplexer was proposed by using T-shaped resonator, ring resonator, and meandered lines. A high-isolation microstrip duplexer designed for radio occultation systems for future planetary systems was presented in paper [13]. In paper [14], a six-channel multiplexers have also been developed. In paper [15], eight-channel diplexer based on stepped impedance resonators and common-input port coupling distribution has been developed. However, the design of planar diplexers with reduced size and wide stopband remains challenging. In this paper, compact microstrip eight-channel diplexer based on quad-band BPF is presented. The proposed diplexer is operating at 2.5/3.3/5.2/6.57 GHz with 3-dB fractional bandwidth of 3/4.5/4/4.6%, respectively, are for channel 1, 2, 5 and 7, respectively, and 3.9/4.65/5.6/7.2 GHz with 3-dB fractional bandwidths of 3/6/4/5%, respectively, are for channel 3, 4, 6 and 8, respectively. The proposed diplexer is based on two quad-band BPFs. Analysis based on even-and odd-mode equivalent circuit is used to determine the fundamental resonant frequencies of quad-mode stepped impedance resonator (QMSIR). Two second-order quad-band BPFs are constructed in order to be combined together with distributed coupling matching circuit for one planar eight-channel diplexer. Compared with the previous works, the proposed diplexer has the reduced number of resonator due to the multimode resonant presented by the resonator, the smaller size ($0.083\lambda^2$) and the larger fractional bandwidth (97%). This concept has been verified by experimental results.

Design procedure of diplexer

Figure 1(a) shows the layout of the proposed eight-channel diplexer, which is based on the QMSIR. The structure of the proposed QMSIR is shown in Fig. 2. Figure 1(b) represents the

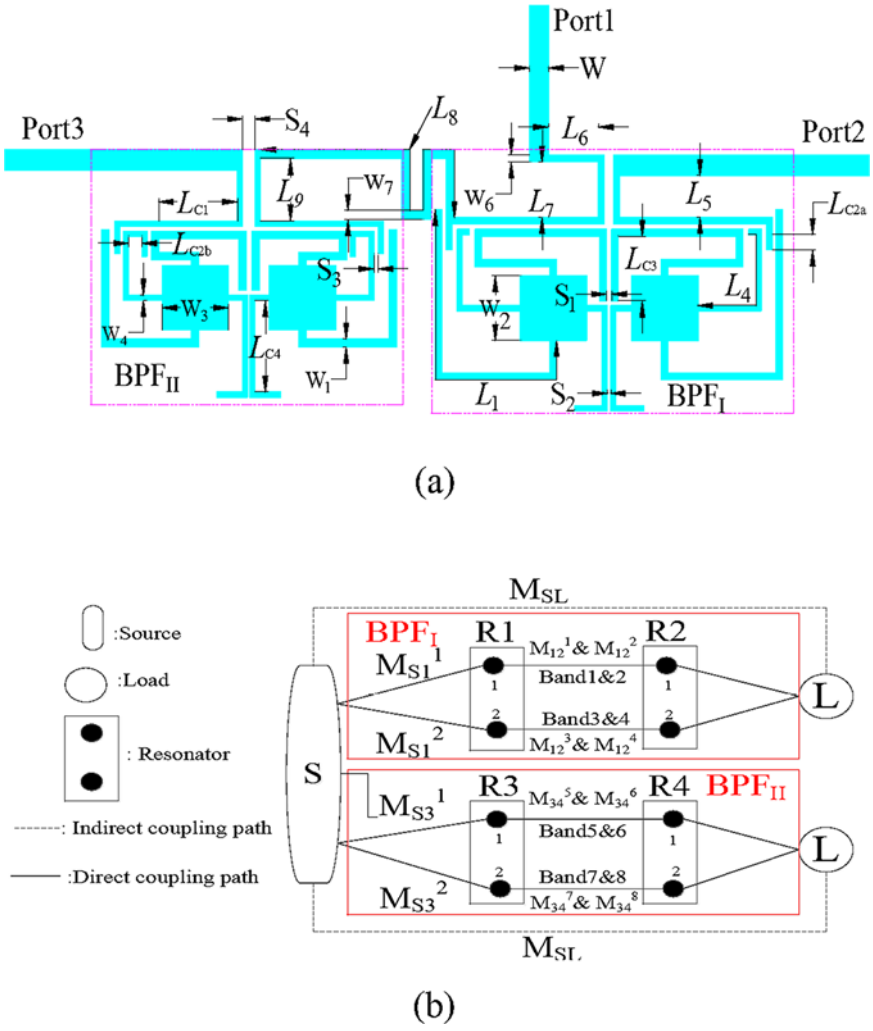

Figure 1. (a) Configuration of the proposed eight-channel diplexer. (b) Its coupling routing topology.

coupling routing diagram of the proposed, where *R* represents a resonator and the solid-lines between notes represent the direct coupling path and the dash-lines between source-load represent the indirect coupling path. *S* and *L* denote the input and output ports, respectively. As it can be seen, the diplexer is formed by two quad-band filters (BPF_I and BPF_{II}), where the BPF_I operates at f_1, f_2, f_5, and f_7, i.e. the center frequencies of the channels 1, 2, 5, and 7, respectively and the BPF_{II} operates at f_3, f_4, f_6, and f_8, i.e. the center frequencies of the channels 3, 4, 6, and 8, respectively.

Characteristics of QMSIR

Figure 2 shows the reported QMSIR with transmission line model (TLM). Its corresponding electrical lengths θ_1, θ_2, θ_3, and θ_4. The design conditions are assumed to be $(\theta_1 + \theta_2) > (\theta_3 + \theta_4)$. The reported resonator is symmetrical, analysis based on even-/odd-mode method is employed. Its corresponding even-/odd-mode equivalent circuits are given in Fig. 3, respectively. At the resonance frequencies, the input impedance (Z_{in}) of each mode will be equal to zero. When plane A-A′ is applied the resonant frequencies can be derived as

$$\tan\theta_2 \tan\theta_1 - R_{Z1} = 0 \rightarrow f_1 \quad (1)$$

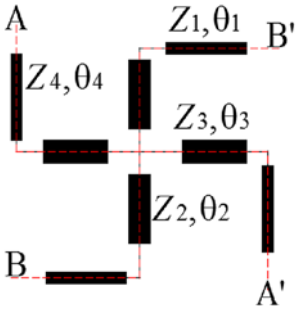

Figure 2. Structure of the proposed QMSIR.

$$R_{Z1}(\tan\theta_4 + R_{Z3}\tan\theta_2) - \tan\theta_1(\tan\theta_2\tan\theta_4 - R_{Z3}) = 0 \rightarrow f_2 \quad (2)$$

Similarly, when plane B-B′ is applied, the resonant frequencies are derived as

$$\tan\theta_3 \tan\theta_4 - R_{Z1} = 0 \rightarrow f_3 \quad (3)$$

$$R_{Z2}(\tan\theta_1 + R_{Z4}\tan\theta_3) - \tan\theta_4(\tan\theta_1\tan\theta_3 - R_{Z4}) = 0 \rightarrow f_4 \quad (4)$$

https://doi.org/10.1017/S1759078724000540 Published online by Cambridge University Press

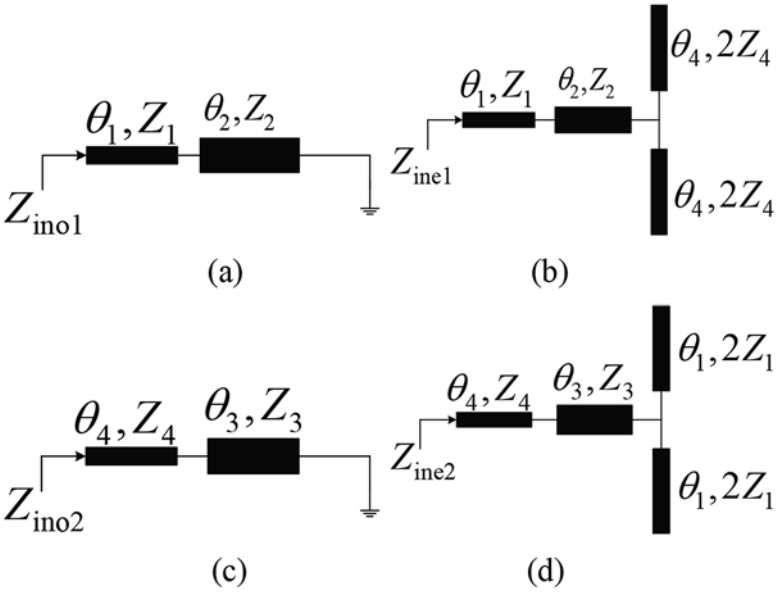

Figure 3. Even-/odd-mode equivalent circuits. (a) and (b) Odd-/even-mode equivalent circuit, respectively, when plane A-A′ is applied. (c) and (d) Odd-/even-mode equivalent circuit, respectively, when plane B-B′ is applied.

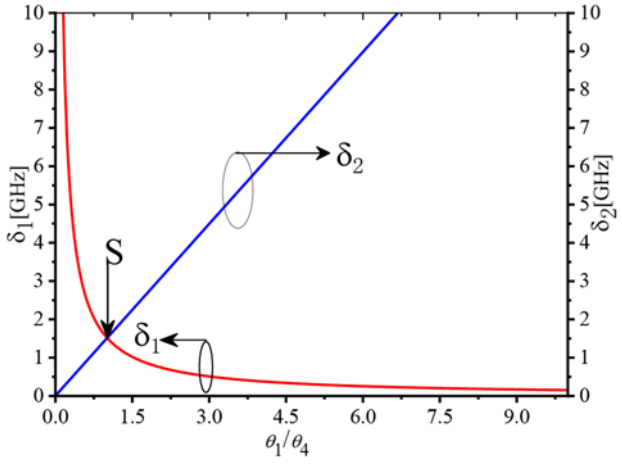

Figure 4. Variation δ_1 and δ_2 with different electrical length ratio θ_1/θ_4 under the condition of $\theta_2 = 11.6^\circ$, $\theta_3 = 27.2^\circ$, $R_{Z1} = 5.95$, and $R_{Z2} = 5.25$.

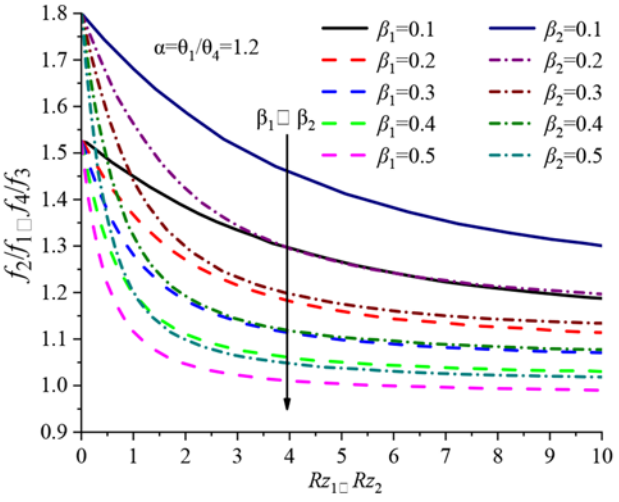

Figure 5. Normalized resonant frequencies of QMSIR against impedance ratios: R_{Z1} with varied β_1 and R_{Z2} with varied β_2. α is fixed to 1.2.

where $R_{Z1} = Z_1/Z_2$, $R_{Z2} = Z_4/Z_3$, $R_{Z3} = Z_4/Z_2$, and $R_{Z4} = Z_1/Z_3$ are the impedance ratios. By defining $\delta_1 = |f_2 - f_1|$ and $\delta_2 = |f_4 - f_3|$, the mode splitting is studied as shown in Fig. 4. As it can be seen in Fig. 4, δ_1 decreases and δ_2 increases as θ_1/θ_4 is increased. At θ_1/θ_4 equals zero, δ_1 tends to large number and δ_2 becomes zero. It suggests that the two resonant frequencies of a f_3 and f_4 will merge. At θ_1/θ_4 tends to large number, δ_1 becomes zero and δ_2 tends to large number. It suggests that two resonant frequencies of a f_1 and f_2 will merge. At point *S*, δ_1 and δ_2 are equal. By adjusting θ_1/θ_4, the quad-mode SIR can provide more freedom to exhibit different characteristics for quad-mode designs. The solutions for θ_1, θ_2, θ_3, and θ_4 are dependent on the choice of impedance ratios R_{Z1} and R_{Z2}, and electrical ratios $\beta_1 = \theta_2/\theta_1 + \theta_2$ and $\beta_2 = \theta_3/\theta_3 + \theta_4$. By properly choosing β_1 and β_2, θ_2 and θ_3 become a function of θ_1 as illustrated in following expressions

$$\theta_2 = \frac{\beta_1}{1-\beta_1}\theta_1 \tag{5}$$

$$\theta_3 = \frac{\beta_2}{1-\beta_2}\theta_1 \tag{6}$$

By normalizing the f_2 to the f_1 and f_4 to the f_3, two normalized resonant frequencies of the QMSIR are obtained as

$$\frac{f_2}{f_1} = \frac{\theta_1 + \theta_2 + \theta_4}{\theta_1 + \theta_2} \tag{7}$$

$$\frac{f_4}{f_3} = \frac{\theta_1 + \theta_3 + \theta_4}{\theta_3 + \theta_4} \tag{8}$$

By introducing the electrical ratios β_1, β_2 and $\alpha = \theta_1/\theta_4$ in equations (7) and (8), the normalized resonant frequencies f_2/f_1 and f_4/f_3 become the function of β_1, β_2, α, R_{Z1}, and R_{Z2} as shown in Fig. 5. As it can be seen in Fig. 5, when the electrical lengths (θ_1 and θ_4) are fixed, varying the impedance ratios (R_{Z1} and R_{Z2}) and electrical ratios (β_1 and β_2), the resonant frequency ratios (f_2/f_1

https://doi.org/10.1017/S1759078724000540 Published online by Cambridge University Press

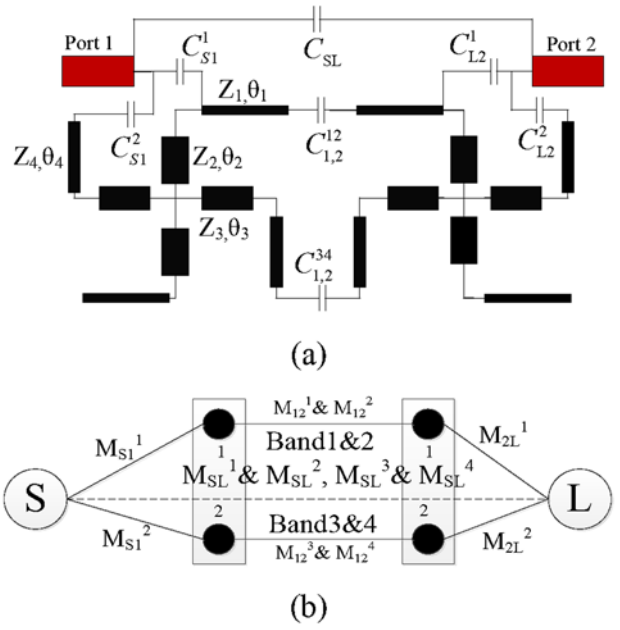

Figure 6. (a) Configuration quad-band BPF using TLM and (b) coupling schematic topology of quad-band BPF.

Table 1. Design coupling coefficients and external quality factors for BPF I and BPF II

	Bandpass		BPF_{II}	BPF_{I}
Coupling coefficients	Band 1	M^1_{12}	0.023	0.023
	Band 2	M^2_{12}	0.034	0.046
	Band 1	$M^1_{S1} = M^1_{2L}$	0.023	0.023
		M^1_{SL}	−0.0054	−0.0054
	Band 2	$M_S1^2 = M^2_{2L}$	0.034	0.046
		M^2_{SL}	−0.008	−0.011
	Band 3	M^3_{12}	0.03	0.03
	Band 4	M^4_{12}	0.035	0.038
	Band 3	$M^3_{S1} = M^3_{2L}$	0.03	0.03
		M^3_{SL}	−0.0072	−0.0072
	Band 4	$M_S1^4 = M^4_{2L}$	0.035	0.038
		M^3_{SL}	−0.0083	−0.009
External quality factor	Band 1	Q^1_e	45.94	45.94
	Band 2	Q^2_e	30.62	22.97
	Band 3	Q^3_e	34.46	34.46
	Band 4	Q^4_e	29.96	27.56

and f_4/f_3) decrease as the electrical length ratios (β_1 and β_2) and impedance ratios (R_{Z1} and R_{Z2}) increase. Based on these characteristics of quad-mode SIR, the design procedures to obtain the quadruple-mode of quad-mode SIR are summarized as follows: (1) Fix the electrical ratio α. (2) Choose the electrical length ratios β_1 and β_2 according to the resonant frequency ratios (f_2/f_1 and f_4/f_3) and determine the impedance ratios (R_{Z1} and R_{Z2}). (3) Fix the value of θ_1 to compute θ_2, θ_3, and θ_4 using equations (5), (6) and electrical length ratio $\alpha = \theta_1/\theta_4$. Then the electrical length parameters are found.

Design of quad-band BPFs

Based on the above analysis, two second-order quad-band BPFs are designed according to the configuration and coupling routing topology shown in Fig. 6. Multiple coupling technique is employed to implement the four passbands. The couplings θ^1_2, Z^1_1, and Z^1_1 are used to generate the passbands f_1 and f_2 while the couplings Z^1_2, θ^1_4, and θ^1_3 are used to generate the passbands f_3 and f_4. By considering $f_{11} = 2.5$ GHz, $f_{21} = 3.3$ GHz, $\alpha = 1.2$, and $\beta_1 = 0.1$, with $f_{21}/f_{11} = 1.32$ and $R_{Z11} = 3.3$, and $f_{31} = 5.2$ GHz, $f_{41} = 6.57$ GHz, $\alpha = 1.2$, and $\beta_2 = 0.2$ with $f_{41}/f_{31} = 1.26$ and $R_{Z21} = 5.1$ for the first quad-band BPF, and $f_{12} = 3.85$ GHz, $f_{22} = 4.65$ GHz, $\alpha = 1.2$, and $\beta_1 = 0.1$ with $f_{22}/f_{12} = 1.21$ and $R_{Z12} = 7.9$, and $f_{32} = 5.6$ GHz, $f_{42} = 7.2$, $\alpha = 1.2$, and $\beta_2 = 0.2$ with $f_{42}/f_{32} = 1.28$ and $R_{Z22} = 5.5$ for the second quad-band BPF, the initial electrical length parameters of the two quad-band BPFs are determined as: (1) for the first quad-band BPF, by taking $\theta^1_1 = 90^\circ$ with $R^1_{Z1} = 3.3\Omega$, the initial values are $\theta^1_2 = 10^\circ$, $Z^1_1 = 87.5\Omega$, $Z^1_2 = 26.5\Omega$, $\theta^1_4 = 75^\circ$ and $\theta^1_3 = 18.75^\circ$, $Z^1_1 = 105.8\Omega$ and $Z^1_2 = 20.75\Omega$. (2) For the second quad-band BPF, by taking $\theta^2_1 = 87.3^\circ$, $R^2_{Z1} = 7.9\Omega$, the initial values are $\theta^2_2 = 9.7$, $Z^2_1 = 82.99\Omega$, $Z^2_2 = 10.5\Omega$, $\theta^2_4 = 72.75$, $\theta^2_3 = 18.18$, $Z^2_1 = 114.61\Omega$, and $Z^2_2 = 20.83\Omega$.

The required coupling coefficients and the external quality factors for BPF I and II are listed in Table 1. Figures 7 and 8 show the coupling coefficient and external quality factor for four passbands of the BPFI and BPFII, respectively. The coupling coefficients and external quality factors are determined by the parameters of the resonators and feeding lines. As it can be seen in Fig. 7, the coupling coefficient decreases as the spacing S_1 and S_2 increase. At a fixed coupled length L_{C3}, the stronger the coupling leads to mode splitting when the spacing S_1 is smaller as shown in Fig. 7(a) and (c). The larger spacing S_1 makes proper coupling for the passbands corresponding to $M^{1,I}_{12}$, $M^{2,I}_{12}$, $M^{1,II}_{12}$, and $M^{2,II}_{12}$. At a fixed length L_{C4}, the weaker the coupling leads to mode splitting when the spacing S_2 is larger, as shown in Fig. 7(b) and (d). The small spacing S_2 makes proper coupling for the passbands corresponding to $M^{3,I}_{12}$, $M^{4,I}_{12}$, $M^{3,II}_{12}$, and $M^{4,II}_{12}$. As it can be observed in Fig. 8, by setting the widths of feeding lines for BPFI and BPFII to 0.3 mm and 0.2 mm, respectively, Q_e for four bands will be increased as the coupled lengths L_{C1} and L_{C2a} increase. For the coupled length L_{C2b}, Q_e for passband 3 will be increased as the L_{C2b} increases while Q_e for passband 4 will be decreased as L_{C2b} increases. As shown in Fig. 9, simulation results of the two quad-band BPFs are obtained. The simulation of the two quad-band BPFs were carried out using Taconic RF-35(tm) tangent of 0.0018. The simulation results for the two substrate with a thickness of 0.508 mm, relative dielectric constant of 3.5, and loss tangent of 0.0018. The simulation results for the two quad-band BPFs show that each quad-band BPF presents four passbands and eight transmission zeros. According to the standard design procedure given in paper [16], the four transmission zeros (TZ2, TZ3, TZ4, and TZ5) are created due to the coupling coefficients MSL1 and MSL2 while the four transmission zeros (TZ6, TZ7, TZ8, and TZ9) are created due to the coupling coefficients MSL3 and MSL4. The extra transmission zero TZ1 in lower stopband is created due to S_4 and L_5. It is easy to see that

https://doi.org/10.1017/S1759078724000540 Published online by Cambridge University Press

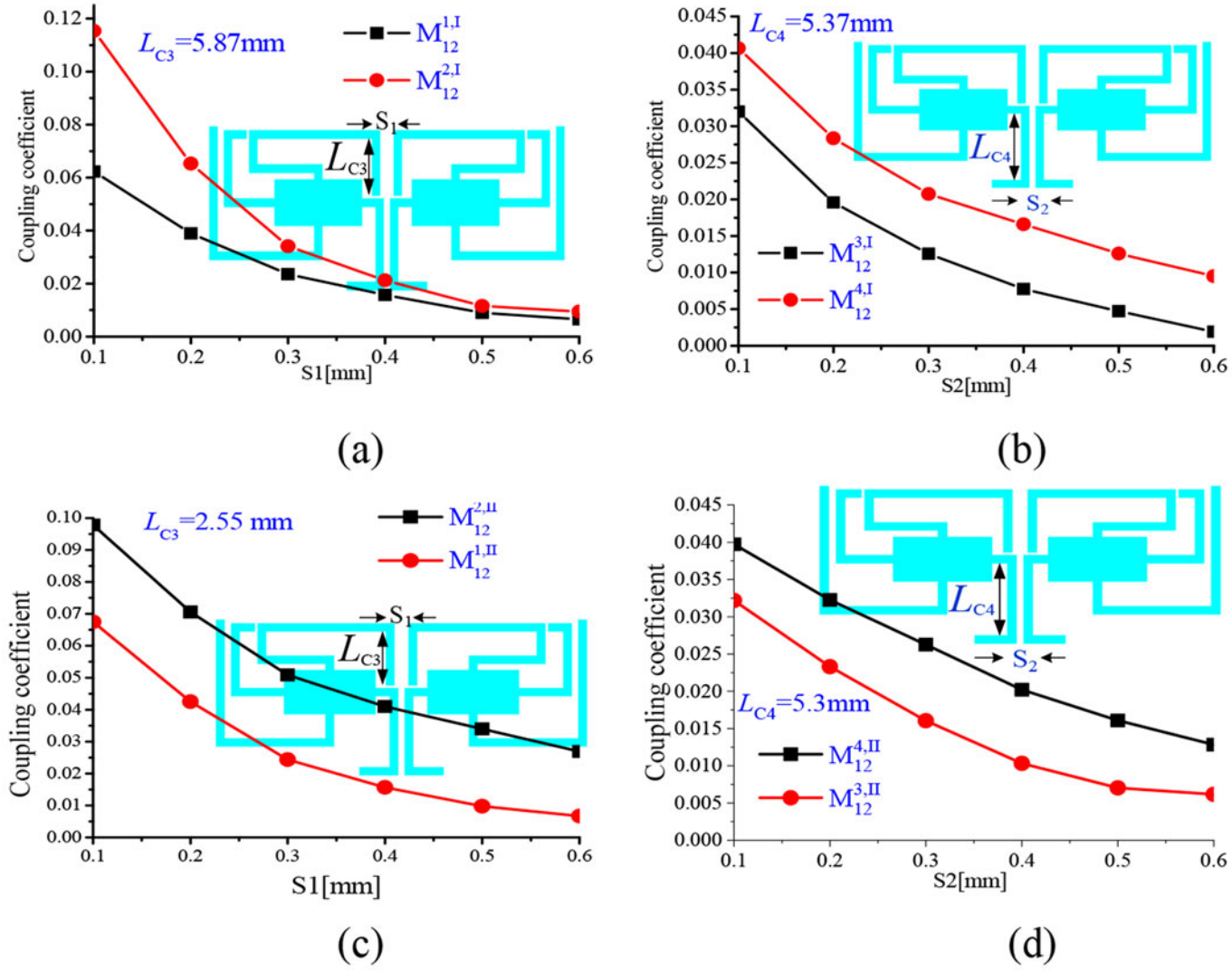

Figure 7. Coupling coefficient BPF I and II. (a) and (c) are coupling coefficients for passband 1 and 2. (b) and (d) are coupling coefficients for passband 3and 4.

around 7.5 GHz, BPF1 has an excess parasitic passband, since the proposed four-bandpass filter BPF1 is based on a cascade of two QMSIRs, it may generate a parasitic passband due to inappropriate size design. However, the filter size is optimized based on the frequency of the four passbands, so the parasitic passband of BPF1 is difficult to eliminate. However, the parasitic passband is eliminated after the cascade of two four-BPFs, mainly because the passband is slightly offset after the cascade, and the overall size is optimized again, thus eliminating the excess parasitic passband.

Design of eight-channel diplexer

Based on the results from the simulation of the two quad-band BPFs, an eight-channel diplexer is realized as shown in Fig. 1(a). The proposed diplexer consists of a distributed coupling feeding line (port 1), two pairs of resonators (R_1 to R_4), and output feeding lines (port 2 and port 3). Basically, there are two unit cells in the proposed diplexer, and each unit cell is a quad-band BPF. The center frequencies of the signals filtered out by each output port are 2.5/3.3/5.2/6.57 GHz and 3.9/4.65/5.6/7.2 GHz for port 2 and port 3, respectively. Each four channels are controlled by a quad-band BPF. The parameters of the proposed diplexer are shown in Table 2. More precisely, design procedures for the proposed diplexer are given as: (1) two quad-band BPFs are designed according to the given passband's specifications. (2) By properly locating the resonators with respect to the distributed coupling feeding line and output feeding lines, the harmonic passband of each quad-band BPF is effectively suppressed to achieve good isolation. (3) Design is finished with some final adjustment in a full-wave simulation. The electrical lengths and impedances of the four parts of the microstrip resonators become asymmetrical after final adjustment to get a good match for the diplexer.

https://doi.org/10.1017/S1759078724000540 Published online by Cambridge University Press

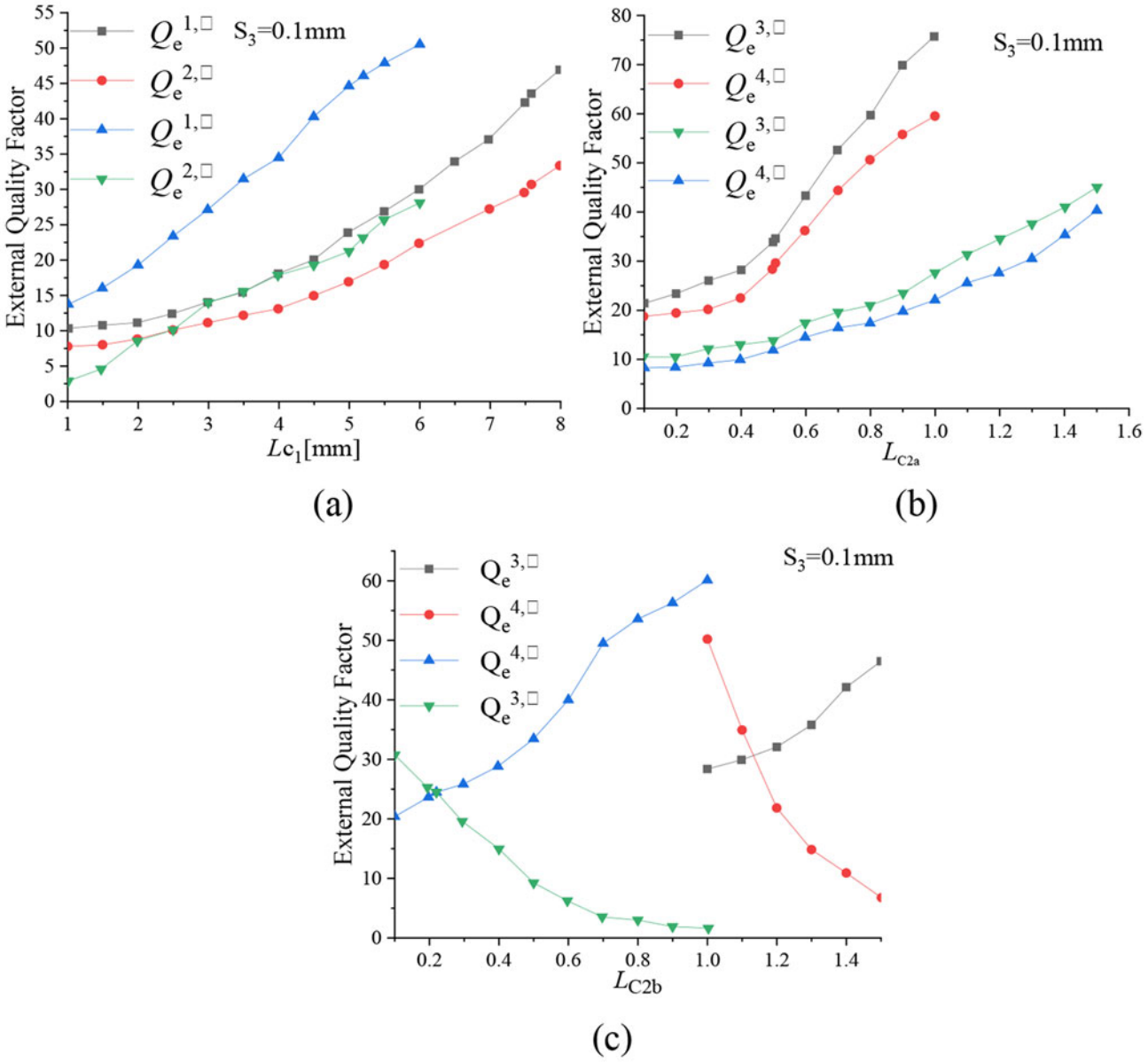

Figure 8. External quality factors of BPF I and BPF II (a) for passband 1 and 2, (b) for passband 3 and 4 with L_{c2a}, and (c) for passband 3 and 4 with L_{c2b}.

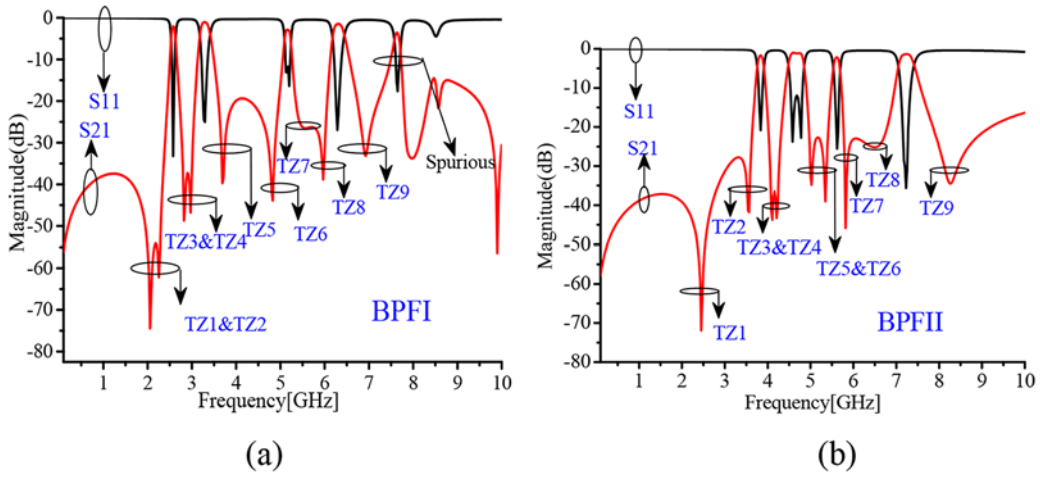

Figure 9. Simulated quad-band bandpass filters (a) for BPF I and (b) for BPF II.

https://doi.org/10.1017/S1759078724000540 Published online by Cambridge University Press

Experimental results

A planar eight-channel diplexer is designed and fabricated on Taconic RF-35(tm) substrate with a thickness of 0.508 mm, relative dielectric constant of 3.5, and loss tangent of 0.0018. The photograph of the fabricated eight-channel diplexer is shown in Fig. 10(b). The measured insertion ($|S_{21}|$ and $|S_{31}|$) and return ($|S_{11}|$) losses of the fractional bandwidths of 3/4.5/3/6/4/4/4.6/5%, respectively. The measured insertion losses, including the losses from SMA connectors, are less than 2/2.6/2.3/1.4/3.9/2.6/1.4/2 dB, respectively, while the measured return losses are greater than 16/10/14/12/15/14/15/14 dB, respectively. The measured isolation $|S_{32}|$ between the passbands is better than 20 dB as shown in Fig. 10(c). Table 3 gives the performance of the proposed diplexer and the previous works. The proposed circuit achieved eight channels, and shows the advantages of compact size and flexibility design with reduced number of resonators in comparison with the

Table 2. Circuit dimensions for diplexer

L_1^I	17.7	L_4^I	8.1	L_5^I	2.35	W	1.15
W_1^I	0.4	W_2^I	4.6	W_3^I	4	W_4^I	0.25
W_5^I	0.35	S_1^I	0.3	S_2^I	0.1	S_3^I	0.1
S_4^I	0.6	L_{C1}^I	7.7	L_{C2}^I	1.35	L_{C3}^I	2.6
L_{C4}^I	5.37	L_1^{II}	12.45	L_4^{II}	7.9	L_5^{II}	2.85
W_1^{II}	0.45	W_2^{II}	4.4	W_3^{II}	3.6	W_4^{II}	0.2
W_5^{II}	0.2	S_1^{II}	0.35	S_2^{II}	0.1	S_3^{II}	0.1
S_4^{II}	0.75	L_{C1}^{II}	5.2	L_{C2}^{II}	0.45	L_{C3}^{II}	2.55
L_{C4}^{II}	5.3	L_6	3	L_7	3.1	L_8	20.65
L_9	3.65	W_6	0.4	W_7	0.35	units: mm	

Table 3. Comparison with the previous works

Ref	L/P	Passband (GHz) Insertion loss (dB)	Iso	RN	Size (λ^2)
[14]	2/6	10/12/19/21/32/35	30	12	4
		2.2/3.1/3.2/2/2.8/3			
[15]	2/8	0.9/1.2/1.5/1.8/2.1/2.4/2.7/3	29	16	0.1
		2.1/2.3/2.4/2.6/2.3/2.2/2.8/2.3			
[17]	4/8	1/1.2/1.4/1.6/1.8/2/2.3/2.6	>30	2	0.088
		2.5/2.1/2.8/2.5/2.7/2.6/2/2			
[18]	3/6	1/1.3/1.6/1.9/2.2/2.5	>33	2	0.384
		2.56/2.1/2.24/2.6/2.652/2.5			
[19]	8/8	0.85/1.05/1.3/1.5/1.65/1.85/2.05/2.3	>27	2	0.105
		2.7/2.4/2.4/3/3.4/3.8/4.2/4.6			
[20]	2/8	1.575/1.8/2.4/2.6/3.5/4.3/5.2/5.7	40	4	0.116
		2.5/2/1.4/1.1/1.8/0.9/2.3/1.5			
[21]	8/8	0.85/1.05/1.3/1.5/1.65/1.85/2.05/2.3	>27	4	0.105
		2.7/2.4/2.4/3/3.4/3.8/4.2/4.6			
[22]	2/8	1.575/1.8/2.4/2.6/3.5/4.2/5.2/5.7	>40	8	0.1
		2.5/2.0/1.4/1.1/1.8/0.9/2.3/1.5			
[23]	4/8	1.0/1.2/1.4/1.6/1.8/2.0/2.3/2.6	>30	4	0.088
		2.5/2.1/2.8/2.5/2.7/2.6/2.0/2.0			
This work	**2/8**	**2.5/3.3/3.9/4.65/5.2/5.5/6.65/7.2**	**>20**	**4**	**0.083**
		2/2.6/2.3/1.4/3.9/2.6/1.4/2			

Note: L = load; P = passband number; Iso = isolation; RN = resonator number.

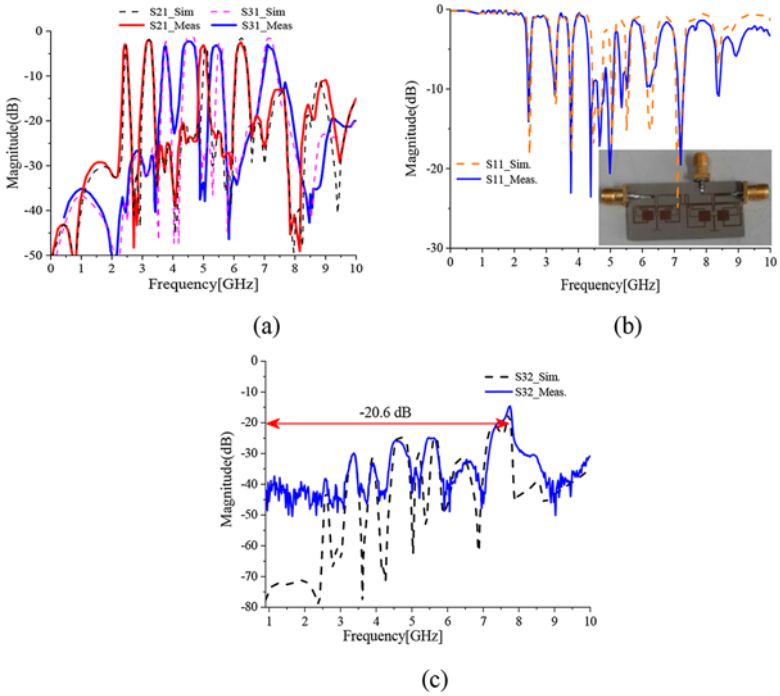

Figure 10. Simulated and measured results of the eight-channel diplexer: (a) and (b) magnitude of S-parameters, and (c) isolation.

https://doi.org/10.1017/S1759078724000540 Published online by Cambridge University Press

previous works shown in Fig. 10(b). The measured insertion ($|S_{21}|$ and $|S_{31}|$) and return ($|S_{11}|$) losses of the fractional bandwidths of 3/4.5/3/6/4/4/4.6/5%, respectively. The measured insertion losses, including the losses from SMA connectors, are less than 2/2.6/2.3/1.4/3.9/2.6/1.4/2 dB, respectively, while the measured return losses are greater than 16/10/14/12/15/14/15/14 dB, respectively. The measured isolation $|S_{32}|$ between the passbands is better than 20 dB as shown in Fig. 10(c). Table 3 gives the performance of the proposed diplexer and the previous works. The proposed circuit achieved eight channels, and shows the advantages of compact size and flexibility design with reduced number of resonators in comparison with the previous works.

Conclusion

A compact eight-channel diplexer based on QMSIR is designed and fabricated. The eight-channel diplexer is achieved due to the two second-order quad-band BPFs. It is worth noting that the size of the design ($0.083\lambda^2$) is smaller than previous ones, which is more conducive to assembly and integration in microwave systems. And the proposed diplexer has reduced number of resonators and larger fractional bandwidth (97%) than previous designs. Good agreement between the simulated results and measured results validates the performance of the proposed diplexer. The proposed compact eight-channel diplexer is particularly suitable for multi-band applications in wireless communication systems.

Data availability statement. All the materials used in the study are mentioned within the article.

Author contributions. Conceptualization, Song K; methodology, software, validation, formal analysis, investigation, resources, and data curation, Fang L; writing – review and editing, visualization, supervision, project administration, and funding acquisition, Zhou Y, Qian Li, and Yong Fan. All authors have read and agreed to the published version of the manuscript.

Funding statement. The work was supported in part by National Natural Science Foundation of China (Grant No: 62171097).

Competing interests. The authors declare no conflicts of interest.

References

1. **Song K, Zhu Y, Zhao M, Fan M and Fan Y** (2017) Miniaturized bandpass filter using dual-mode hexagonal loop resonator. *International Journal of Microwave and Wireless Technologies* **9**(5), 1003–1008.
2. **Hong J-S and Lancaster MJ** (2004) *Microstrip Filters for RF/Microwave Applications*. John Wiley & Sons.
3. **Chi P-L, Hsieh H-Y and Yang T** (2022) 28-GHz high-isolation SIW balanced diplexer with highly controllable transmission zeros. *IEEE Transactions on Circuits and Systems II: Express Briefs* **69**(12), 4799–4803.
4. **Liu B-G and Cheng C-H** (2022) Compact triple-mode folded-HMSIW diplexer with wide stopband and high isolation based on embedded isolation network. *IEEE Transactions on Circuits and Systems II: Express Briefs* **69**(11), 4298–4302.
5. **Song K, Luo M, Zhong C, Chen Y, Zhou Y and Xia F** (2021) Compact multimode-resonator multiplexer with wide upper-stopband and high isolation. *International Journal of Microwave and Wireless Technologies* **13**(2), 111–118.
6. **Li WT, Zhang HR, Chai XJ, Mou JC, Hei YQ and Shi XW** (2023) Novel unbalanced-to-balanced quad-channel diplexer with controllable bandwidth and high isolation. *IEEE Transactions on Circuits and Systems II: Express Briefs* **70**(4), 1281–1285.
7. **Chan KYE and Ramer R** (2015) Millimeter-wave reconfigurable bandpass filters. *International Journal of Microwave and Wireless Technologies* **7**(6), 671–678.
8. **Song K, Luo M, Zhong C and Chen Y** (2020) High-isolation diplexer based on dual-mode substrate integrated waveguide resonator. *International Journal of Microwave and Wireless Technologies* **12**(4), 288–292.
9. **Kaddour D, Arnould J-D and Ferrari P** (2009) A semi-lumped microstrip UWB bandpass filter. *International Journal of Microwave and Wireless Technologies* **1**(1), 57–64.
10. **Chen F, Song K, Hu B and Fan Y** (2014) Compact dual-band bandpass filter using HMSIW resonator and slot perturbation. *IEEE Microwave and Wireless Components Letters* **24**(10), 686–688.
11. **Hammed RT** (2022) Multilayered U-shape diplexer for high performance multifunctional wireless communication systems *AEU-International Journal of Electronics and Communications* **150**, 154217.
12. **Bavandpour SK, Roshani S, Pirasteh A, Roshani S and Seyedi H** (2021) A compact lowpass-dual bandpass diplexer with high output ports isolation. *AEU-International Journal of Electronics and Communications* **135**, 153748.
13. **Upadhyaya T, Pabari J, Sheel V, Desai A, Patel R and Jitarwal S** (2020) Compact and high isolation microstrip diplexer for future radio science planetary applications. *AEU-International Journal of Electronics and Communications* **127**, 153497.
14. **Seungpyo Hong and Kai Chang**, "A 10-35-GHz six-channel microstrip multiplexer for wide-band communication systems," in *IEEE Transactions on Microwave Theory and Techniques*, vol. **54**, no. 4, pp. 1370–1378, June 2006
15. **Tu W-H and Hung W-C** (2014) Microstrip eight-channel diplexer with wide stopband. *IEEE Microwave and Wireless Components Letters* **24**(11), 742–744.
16. **Denis B, Song K and Zhang F** Compact dual-band bandpass filter using open stub-loaded stepped impedance resonator with cross-slots, International Journal of Microwave and Wireless Technologies, pp. 1–6.
17. **Kumar Jhariya D, Mohan A, Kaushik R and Saxena VN** (2020) Circular-shaped differential wideband band pass filter. *International Journal of Microwave and Wireless Technologies* **12**(3), 193–197.
18. **Hsu H-W and Tu W-H** (2017) Microwave microstrip six-channel triplexer and eight-channel quadruplexer. *IEEE Transactions on Components, Packaging and Manufacturing Technology* **7**(7), 1136–1143.
19. **Yahya SI and Nouri L** (2021) A low-loss four-channel microstrip diplexer for wideband multi-service wireless applications. *AEU-International Journal of Electronics and Communications* **133**, 153670.
20. **Dong G, Li S and Yang X** (2022) A tunable bandpass filter with extended passband bandwidth. *International Journal of Microwave and Wireless Technologies* **14**(10), 1233–1240.
21. **Chen CF, Tseng BH, Wang GY and Li JJ** (2018) Compact microstrip eight-channel multiplexer with independently switchable passbands. *IET Microwaves, Antennas & Propagation* **12**(6), 1026–1033.
22. **Chen Y-W, Wu H-W, Chiu C-T and Su, YK** (2018) Design of new eight-channel diplexer for multiband wireless communication system. *IEEE Access* **6**, 49732–49739.
23. **Tseng BH, Chang SF, Lin CY and Chen CF** A compact eight-channel microstrip quadruplexer using quad mode stub-load resonators. Asia-Pacific Microwave Conference. IEEE, 2014: 7–9.

https://doi.org/10.1017/S1759078724000540 Published online by Cambridge University Press

Kaijun Song (M'09-SM'12) received the M.S. degree in radio physics and the Ph.D. degree in electromagnetic field and microwave technology from the University of Electronic Science and Technology of China (UESTC), Chengdu, China, in 2005 and 2007, respectively. Since 2007, he has been with the EHF Key Laboratory of Science, School of Electronic Engineering, UESTC, where he is currently a full Professor. From 2007 to 2008, he was a postdoctoral research fellow with the Montana Tech of the University of Montana, Butte, USA, working on microwave/millimeter-wave circuits and microwave remote sensing technology. From 2008 to 2010, he was a research fellow with the State Key Laboratory of Millimeter Waves of China, Department of Electronic Engineering, City University of Hong Kong, on microwave/millimeter-wave power-combining technology and ultra-wideband (UWB) circuits. He was a senior visiting scholar with the State Key Laboratory of Millimeter Waves of China, Department of Electronic Engineering, City University of Hong Kong in November 2012. He has published more than 90 internationally refereed journal papers. His current research fields include microwave and millimeter-wave/THz power-combining technology; UWB circuits and technologies; microwave/millimeter-wave devices, circuits and systems; and microwave remote sensing technologies. Prof. Song is the reviewer of tens of international journals, including IEEE Transactions and IEEE Letters.

Lele Fang was born in Henan, China, 2000. He received the B.Sc. degree in Industrial Engineering from the Zhengzhou University in 2023. Now he is trying to obtain his master degree in electrical engineering in University of Electronic Science and Technology of China (UESTC). His current research interests include microwave/millimeter-wave power-combining technology and micromillimeter-wave techniques with a focus in RF/microwave passive circuits and systems.

Qian Li was born in Hefei, China, in 1995. She received the B.Sc. degree in Electronic Science and Technology from the Anhui University in 2018. She is currently pursuing the Ph.D. degree in the University of Electronic Science and Technology of China. Her current research interests include microwave power dividers/combiners and reconfigurable circuits.

Yong Fan received a B.E. degree from Nanjing University of Science and Technology, Nanjing, Jiangsu, China, in 1985, and a M.S. degree from University of Electronic Science and Technology of China, Chengdu, Sichuan, China, in 1992. He is a senior member of Chinese Institute of Electronics. From 1985 to 1989, he was interested in microwave integrated circuits. Since 1989, his research interests include millimeter-wave communication, electromagnetic theory, millimeter-wave technology, and millimeter-wave systems. He has authored or coauthored over 90 papers, 30 of which are searched by SCI and EI.

https://doi.org/10.1017/S1759078724000540 Published online by Cambridge University Press